JOURNAL OF AIRCRAFT
Vol. 32, No. 1, January–February 1995

Effect of Curvature in the Numerical Simulation of an Electrothermal De-Icer Pad

J. R. Huang,* Theo G. Keith Jr.,† and Kenneth J. De Witt‡
University of Toledo, Toledo, Ohio 43606

A finite element method, which incorporates an assumed phase state technique, is presented for the solution of one- and two-dimensional heat conduction problems with phase change. A simulation of an electrothermal de-iced aircraft surface is made using this method. The major interest of this study is the effect of the surface curvature on the numerical results. Comparison of predicted temperatures within a rectangular simulation and those within an airfoil reveals the extent and importance of modeling curvature effects. When surface curvature is less than 0.25, curvature effects may be neglected and a rectangular shape may be used instead of the actual geometry.

Nomenclature

A = global matrix of linear system of equations
a, b, c = element geometry coefficients
C^* = apparent heat capacity
C_T = dimensionless coefficient in Kirchhoff temperature function
c = specific heat capacity
E = element area
H = enthalpy per unit volume
h = heat-transfer coefficient
K = curvature
K_1 = mass matrix
K_2 = boundary condition matrix
K_3 = thermal condition matrix
k = thermal conductivity
L = elemental side length
m_1 = total node number
$\boldsymbol{n}$ = unit normal vector
$\boldsymbol{P}$ = global vector of linear system of equations
$\boldsymbol{P}_1$ = heat source vector
$\boldsymbol{P}_2$ = boundary condition vector
q = rate of heat generation per unit volume
T = temperature
T_∞ = ambient temperature
t = time
x, y = node coordinates
α, β = boundary condition coefficients
Δt = time step
θ = Kirchhoff variable
ρ = density

Subscripts
i, j, k = nodal indices of a triangular element
R = reference value

Superscripts
n = time level
0 = initial condition

Received May 14, 1992; revision received May 2, 1994; accepted for publication May 3, 1994. Copyright © 1994 by the American Institute of Aeronautics and Astronautics, Inc. All rights reserved.

*Graduate Student, Mechanical Engineering Department.
†Distinguished University Professor, Mechanical Engineering Department. Associate Fellow AIAA.
‡Distinguished University Professor, Chemical Engineering Department.

Introduction

THE removal and/or prevention of ice on aircraft components, e.g., wing surfaces, nacelles, inlets, etc., is vital to aircraft performance and operation. Even small amounts of ice can have disastrous consequences. Methods of ice control can be arranged into two broad categories: 1) anti-icing methods and 2) de-icing methods. Anti-icing methods are concerned with the prevention or minimization of ice buildup on exposed surfaces. Anti-icing systems generally utilize chemical or thermal principles. De-icing methods are concerned with ice removal during and after ice buildup. De-icing systems generally utilize mechanical or thermal principles.

An electrothermal de-icer pad is a widely used thermal de-icing system. By this method of wing surface ice control, heater pads are installed beneath the skin surrounding the leading edge, as shown in Fig. 1. The heaters are activated during icing conditions to remove any accreted ice. Electrical energy in the form of conducted heat destroys the adhesion forces at the ice-wing surface interface. Aerodynamic forces are then able to sweep the ice from the surface.

The complexity associated with the airfoil geometry and the phase change of the ice require that a numerical technique be used to simulate an electrothermally de-iced aircraft surface. However, there are three basic difficulties involved with a numerical simulation of a de-icer pad: 1) the curved geometry, 2) the layered structure, and 3) the extremely small layer thicknesses compared to the overall airfoil thickness and chord length. A variety of numerical studies of a de-icer pad have been performed over the past few years, e.g., Refs. 1–4. The numerical approach used in these studies is a transient finite difference technique. The irregular geometry and layered composite materials that are involved make these techniques difficult to apply. Accordingly, most of the previous studies have focused on a rectangular geometry. Recently, Huang et al.[5,6] combined an enthalpy method with a finite

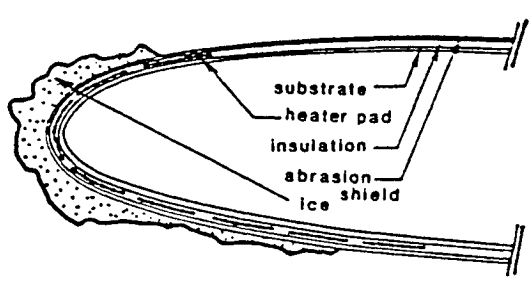

Fig. 1 Airfoil with electrothermal thermal de-icer pad.

Table 1 Data for a typical de-icer pad

Layer	Thickness, in.	Thermal conductivity, btu/h-ft-°F	Diffusivity, ft²/h
Stainless steel abrasion shield	0.0300	8.70	0.1500
Epoxy/glass insulation	0.0388	0.22	0.0087
Copper heater element	0.0065	60.00	1.1500
Expoxy/glass insulation	0.1544	0.22	0.0087
Stainless steel blade skin	0.0300	8.70	0.1500
Aluminum doubler	0.0600	102.00	2.8300
Aluminum substrate	0.1750	102.00	2.8300

element technique (FEM) to simulate a two-dimensional electrothermally de-iced aircraft surface. However, FEM usually takes more CPU time than do comparable finite difference methods. Also, the data input and output for FEM are more involved. On the other hand, it has been reported[1-4] that the finite difference techniques can provide very good approximations compared to experimental data by using simplified rectangular geometry instead of the actual curved de-icer pad configuration. Of course such simplifications are valid only when the curvature of the geometry is negligible. Moreover, if geometry effects are unimportant, then it seems unnecessary to introduce FEM to simulate airfoil geometries since these methods require higher computer costs. At this point, when to utilize FEM in de-icer pad simulations is still in question.

To resolve this question, the effect of curvature on de-icer pad numerical simulation will be carefully examined. First, the simulation results of an actual curved geometry and those of a rectangular simulation will be compared under the same test conditions. Next, a series of cylinders whose compositions and physical properties are the same as those of a standard de-icer pad except for the constant surface curvatures will be analyzed to isolate curvature effects. These comparisons should permit the following questions to be answered:

1) Does surface curvature affect a de-icer pad simulation?

2) If it does, how is the effect connected to the value of the curvature? Conclusions about the effect of the curvature on the de-icer pad simulation may be drawn from these comparisons.

Analysis

Physical Considerations

Geometric and thermal property data for the composite structure investigated in this study are presented in Table 1. The structure consists of seven layers plus a layer of accreted ice. The bottom layer is the load-carrying substrate. The exposed surface of the substrate is subjected to a convective heat exchange. The internal surface of the substrate is covered with a layer of insulation. The heater is sandwiched between two layers of insulation. The bottom insulating layer is much thicker than that of the top layer, so that most of the generated heat is directed towards the ice. A protective metal abrasion shield covers the top layer of insulation. The insulating layers electrically isolate the heater from the metal substrate and the abrasion shield. The layers of the composite are joined to each other with adhesive whose effect will not be considered in this study. The heater is usually very thin (approximately 1/1000–5/1000 in. thick). The ice surface, exposed to the ambient, is subjected to a convective heat exchange that is different from that of the substrate.

Analytical Considerations

The following assumptions were made in the development of a mathematical model for heat conduction in the composite geometry described above:

1) The ambient temperature, inside air temperature, and all heat transfer coefficients are constant with respect to time.

2) There is perfect thermal contact between each layer.

3) The density change due to melting is negligible, i.e., the effect of ice volume contraction during melting is neglected.

4) All materials are isotropic.

The general heat conduction equation is

$$(\rho c)\frac{\partial T}{\partial t} = \nabla\cdot(k\nabla T) + q \tag{1}$$

This expression can be used to determine the temperature distribution within any of the layers including that of the ice. The heat source term q is nonzero only for the heaters.

The initial condition is

$$T = T^{\circ} \quad \text{at} \quad t = 0$$

The convective heat transfer boundary condition for either the bottom surface of the substrate or the ice layer-ambient interface is

$$-k\nabla T\cdot \boldsymbol{n} = h(T - T_{\infty})$$

This can be written more generally as

$$k\nabla T\cdot \boldsymbol{n} + \alpha T + \beta = 0 \tag{2}$$

where $\boldsymbol{n}$ is the unit vector normal to the heat exchange surface. Comparing the above two expressions reveals that $\alpha = h$ and $\beta = -hT_{\infty}$.

The enthalpy method is used to determine the phase change within the ice, and the method of assumed states[7] will be used to describe the latent heat absorption. Equation (1) may be written in terms of the enthalpy per unit volume as

$$\frac{\partial H}{\partial t} = \nabla\cdot(k\nabla T) + q \tag{3}$$

where $dH = \rho c\, dT$. This equation can be applied in both the composite material and the ice since the composite material can be treated as a phase change material that will always be in the solid state.

Equation (3) is nonlinear, due to the dependence of thermal conductivity on temperature, i.e., $k = k(T)$. This difficulty can be circumvented by applying the Kirchhoff transformation

$$\theta = \frac{1}{k_R}\int_{T_R}^{T(X,t)} k(T)\, dT \tag{4}$$

where k_R is an arbitrary reference value of the thermal conductivity. Integrating Eq. (4) using Leibnitz's rule gives

$$\nabla\theta = [k(T)/k_R]\nabla T$$

Introducing this expression into Eq. (3) produces the following linear form:

$$\frac{\partial H}{\partial t} - k_R\nabla^2\theta = q \tag{5}$$

Introducing phase change coefficients θ_R, C_T, H_R, and C^*, and using standard FEM schemes, yields the following results[5,6]:

$$([K_1] + [K_2])^{n+1}[\theta_R + C_T T]^{n+1} + [K_3]^{n+1}[H_R + C^*T]^{n+1} = [K_3]^n[H_R + C^*T]^n + [P_1]^{n+1} - [P_2]^{n+1} \quad (6)$$

or

$$([K_1] + [K_2])^{n+1}[C_T T]^{n+1} + [K_3]^{n+1}[C^*T]^{n+1} = ([K_3]^n[H_R]^n - [K_3]^{n+1}[H_R]^{n+1}) - ([K_1] + [K_2])^{n+1}[\theta_R]^{n+1} + [K_3]^n[C^*T]^n + [P_1]^{n+1} - [P_2]^{n+1} \quad (7)$$

Assuming that the boundary condition will not be affected by phase change, Eq. (7) can be simplified to

$$([K_3C^*]^{n+1} + [K_1C_T]^{n+1} + [K_2C_T]^{n+1})[T]^{n+1} = [K_3C^*]^n[T]^n + [K_3H_R]^n - [K_3H_R]^{n+1} - [K_1]^{n+1}[\theta_R]^{n+1} + [P_1]^{n+1} - [P_2]^{n+1} \quad (8)$$

To avoid numerical integration in the procedure of forming the element matrix, a triangular element has been chosen in this study. Using a triangular element in Eq. (8) results in the following expression for two-dimensional problems:

$$\begin{bmatrix} \frac{\alpha_{ij}L_{ij}}{3} + \frac{\alpha_{ki}L_{ki}}{3} & \frac{\alpha_{ij}L_{ij}}{6} & \frac{\alpha_{ki}L_{ki}}{6} \\ \frac{\alpha_{ij}L_{ij}}{6} & \frac{\sigma_{ij}L_{ij}}{3} + \frac{\alpha_{jk}L_{jk}}{3} & \frac{\alpha_{jk}L_{jk}}{6} \\ \frac{\alpha_{ki}L_{ki}}{6} & \frac{\alpha_{jk}L_{jk}}{6} & \frac{\alpha_{jk}L_{jk}}{3} + \frac{\alpha_{ki}L_{ki}}{3} \end{bmatrix} \begin{bmatrix} T_i^{n+1} \\ T_j^{n+1} \\ T_k^{n+1} \end{bmatrix} + [B] \begin{bmatrix} C_{Ti}^{n+1}T_i^{n+1} \\ C_{Tj}^{n+1}T_j^{n+1} \\ C_{Tk}^{n+1}T_k^{n+1} \end{bmatrix} + \frac{E}{12\Delta t} \begin{bmatrix} 2 & 1 & 1 \\ 1 & 2 & 1 \\ 1 & 1 & 2 \end{bmatrix} \begin{bmatrix} C_i^{*n+1}T_i^{n+1} \\ C_j^{*n+1}T_j^{n+1} \\ C_k^{*n+1}T_k^{n+1} \end{bmatrix}$$
$$= -[B] \begin{bmatrix} \theta_{Ri}^{n+1} \\ \theta_{Rj}^{n+1} \\ \theta_{Rk}^{n+1} \end{bmatrix} + \frac{E}{12\Delta t} \begin{bmatrix} 2 & 1 & 1 \\ 1 & 2 & 1 \\ 1 & 1 & 2 \end{bmatrix} \begin{bmatrix} C_i^{*n}T_i^n + H_{iR}^n - H_{iR}^{n+1} \\ C_j^{*n}T_j^n + H_{jR}^n - H_{jR}^{n+1} \\ C_k^{*n}T_k^n + H_{kR}^n - H_{kR}^{n+1} \end{bmatrix} - \frac{1}{2} \begin{bmatrix} \beta_{ij}L_{ij} + \beta_{ki}L_{ki} \\ \beta_{ij}L_{ij} + \beta_{kj}L_{kj} \\ \beta_{jk}L_{jk} + \beta_{ki}L_{ki} \end{bmatrix} + \frac{E}{3} \begin{bmatrix} q_i \\ q_j \\ q_k \end{bmatrix} \quad (9)$$

where

$$[B] = \begin{bmatrix} \frac{k}{4A}b_i^2 + \frac{k}{4A}c_i^2 & \frac{k}{4A}b_ib_j + \frac{k}{4A}c_ic_j & \frac{k}{4A}b_ib_k + \frac{k}{4A}c_ic_k \\ \frac{k}{4A}b_ib_j + \frac{k}{4A}c_ic_j & \frac{k}{4A}b_j^2 + \frac{k}{4A}c_j^2 & \frac{k}{4A}b_jb_k + \frac{k}{4A}c_jc_k \\ \frac{k}{4A}b_ib_k + \frac{k}{4A}c_ic_k & \frac{k}{4A}b_jb_k + \frac{k}{4A}c_jc_k & \frac{k}{4A}b_k^2 + \frac{k}{4A}c_k^2 \end{bmatrix}$$

Constants a, b, and c are determined from

$$\begin{bmatrix} a_i & a_j & a_k \\ b_i & b_j & b_k \\ c_i & c_j & c_k \end{bmatrix} = \begin{bmatrix} x_jy_k - x_ky_j & x_ky_i - x_iy_k & x_iy_j - x_jy_i \\ y_j - y_k & y_k - y_i & y_i - y_j \\ x_k - x_j & x_i - x_k & x_j - x_i \end{bmatrix}$$

Equation (9) can then be assembled into an $m_1 \times m_1$ linear system of equations

$$[A][T]^{n+1} = [P] \quad (10)$$

The choice of a solver of Eq. (10) is critical since the system of equations is generally very large for an airfoil simulation. In this study an improved lower and upper triangular matrix factorization method was applied. As a result, the CPU time was reduced from 20 to 100 times over the successive over-relaxation method or the Gauss-Siedel method.[6]

Results and Discussion

A computer program was written and run for one- and two-dimensional problems, and, for purposes of validation, the results were compared with existing numerical and experimental data. The details of the comparison have been presented and discussed in Refs. 5 and 6. In this study, major interest will be directed towards using Eq. (8) to simulate two-dimensional de-icer pads that have the same layer structure, physical properties, and test conditions, i.e., 1) all test models are eight layers, which includes the ice layer, (all epoxy adhesive layers have been neglected), physical property information for each layer is given in Table 1; 2) four heaters are modeled, each heater element is 1 in. wide and the gap between heaters is 0.061 in., a constant heater power of 30 W/in.^{2} is used throughout; 3) initial temperatures are set at 20°F; and 4) the outer and inner convection coefficients are 150, and 10 Btu/h-ft^2-°F, respectively. Since all structure, physical properties, and test conditions have been set, the only difference for the test problems is the geometric shape and the surface curvature. In this way, the effects of shape and curvature will become apparent from the differences in results for the various test problems.

Rectangle vs Airfoil Simulation

First, a comparison will be made between the results obtained by modeling a de-icer pad as a rectangle and by modeling it using the actual airfoil geometry. The original rectangle and airfoil input models are shown in Figs. 2 and 3, respectively. The FEM mesh for the rectangle de-icer model (Fig. 2) and the airfoil de-icer model (Fig. 3) are shown in Figs. 4 and 5, respectively.

The temperature histories of interfacial nodes that are positioned at the ice-abrasion shield interface for the rectangular and airfoil geometries are shown in Figs. 6–9. Figures 6 and 7 are plots of temperature vs time for all the nodes at the ice-abrasion shield interface for the rectangular and airfoil geometries, respectively. Figures 8 and 9 are plots showing the temperature at the stagnation point (labeled node 11 and node 18 in Figs. 2 and 3) and the leftmost point (labeled node 1 in Figs. 2 and 3) at the shield interfaces. The differences between treating the de-icer pad as a rectangle and treating it as an airfoil may be listed as follows:

1) Figure 6 is a plot of the temperatures for all the nodes along the interface. But only a few data lines are shown in the plot. The reason for this is that many nodes have nearly the same temperature history for the rectangular simulation

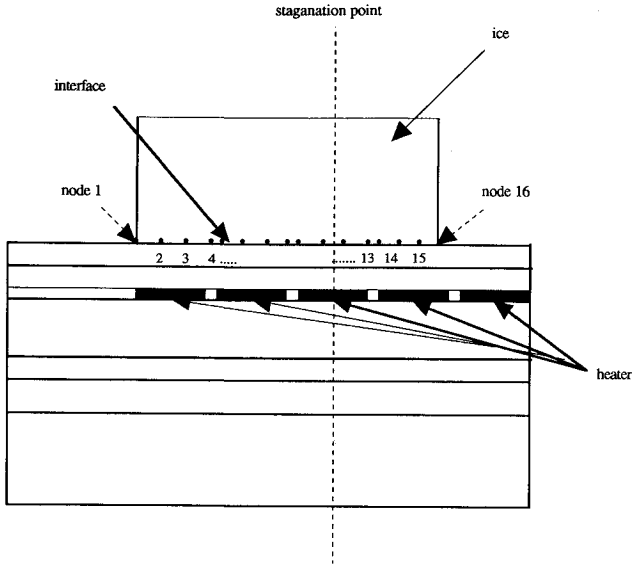

Fig. 2 Rectangle de-icer configuration.

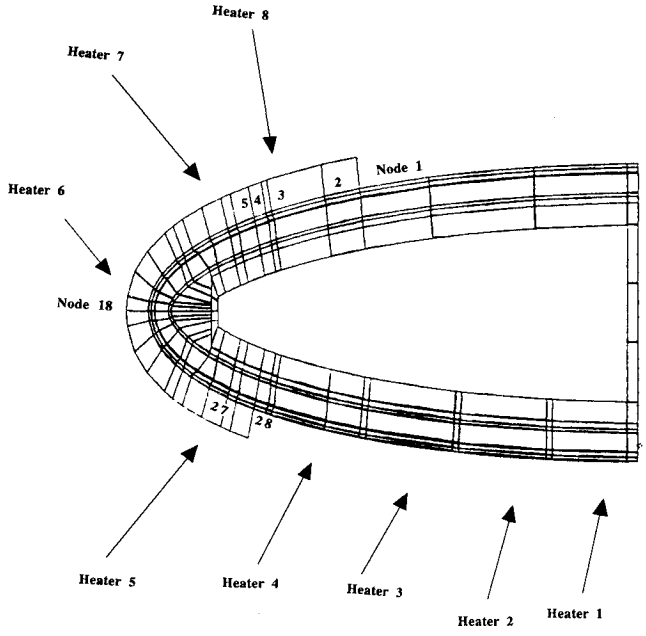

Fig. 3 Airfoil de-icer configuration.

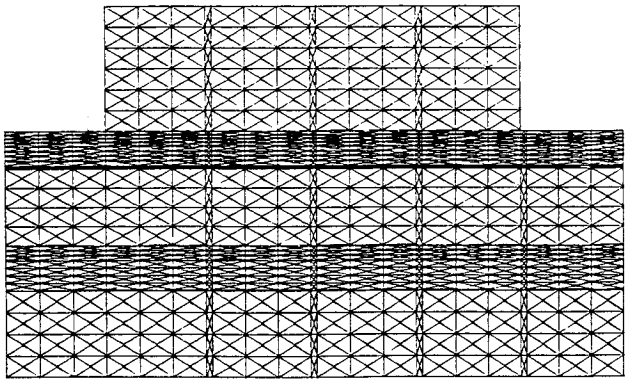

Fig. 4 FEM mesh for rectangle de-icer configuration (for positions of heater pads and nodes refer to Fig. 2).

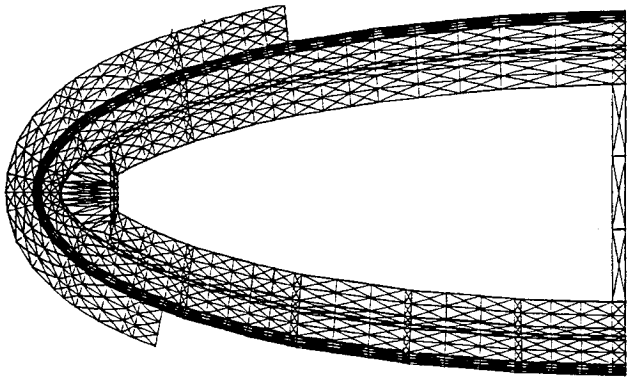

Fig. 5 FEM mesh for airfoil de-icer configuration (for positions of heater pads and nodes refer to Fig. 3).

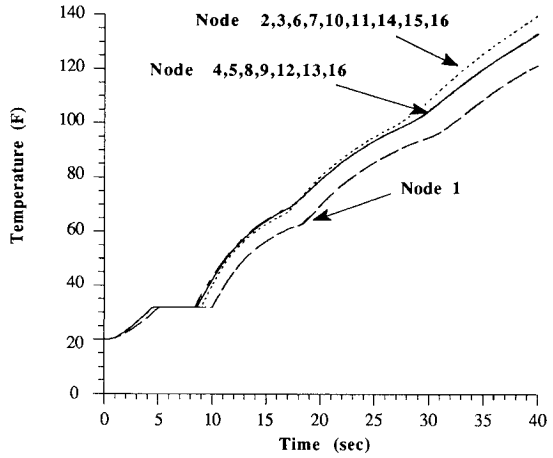

Fig. 6 Temperature history for all rectangular interface nodes.

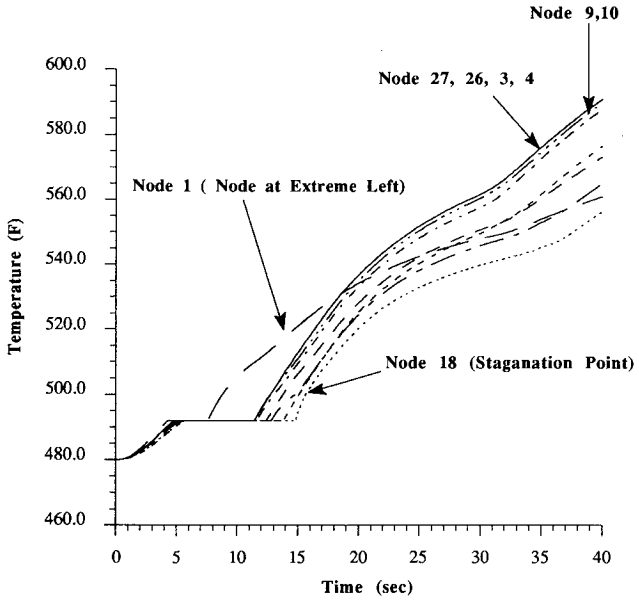

Fig. 7 Temperature history for all airfoil interface nodes.

at the interface and, consequently, they all fall nearly on the same line. On the other hand, many temperature-time lines are shown in the Fig. 7. This indicates that the temperature histories of the interfacial nodes for an actual curved airfoil geometry are quite different from each other, and the nodal temperatures on the interface show a more complicated behavior than do temperatures of the interface for the rectangle case.

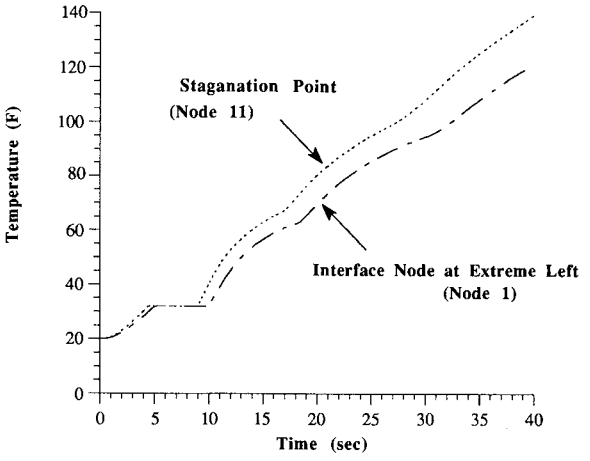

Fig. 8 Temperature history for selected nodes at interface of rectangle.

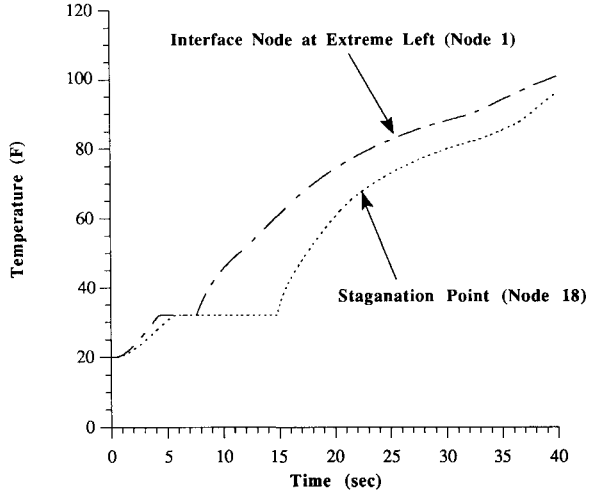

Fig. 9 Temperature history for selected nodes at interface of airfoil.

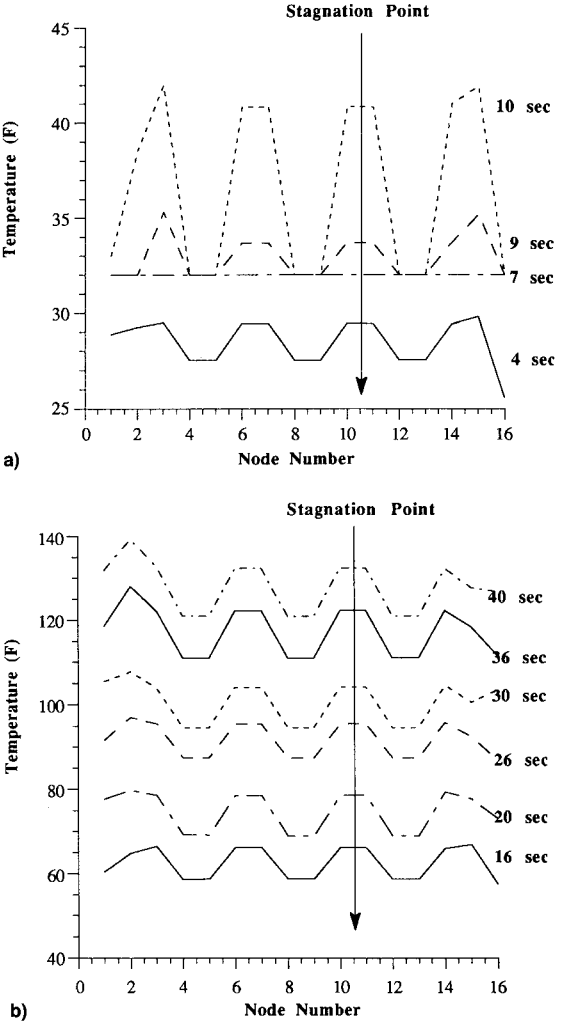

Fig. 10 Temperature profile for interfacial nodes of rectangle for time a) 0–10 and b) 0–40 s.

2) At any specific time, the temperature range (Fig. 7) at the interface (maximum nodal temperature minus minimum nodal temperature) for the airfoil geometry is much larger than the temperature difference (Fig. 6) at the interface for the rectangular geometry.

3) Comparing Fig. 6 to Fig. 7, it can be seen that the flat parts (which denote a two phase region), in both plots start almost at the same time. But the flat portion of the curve for the airfoil lasts about 5 s longer than that in the rectangle simulation. This indicates that the start time of the melting for the interfacial nodes in an airfoil simulation does not differ much from that in a rectangle simulation. However, the time of completing the phase change from ice to water at the interface for an airfoil simulation is considerably longer than in a rectangle simulation.

4) From Fig. 8, the temperature of the stagnation point (node 11 in Fig. 2) for a rectangle simulation is always higher than the leftmost node (node 1 in Fig. 2) at the shield interface and the phase change starting and completion times occur sooner at the stagnation point than at the leftmost node. But Fig. 9 presents a totally different picture: the stagnation point (node 18 in Fig. 3) temperature for an airfoil simulation is always lower than the leftmost node (node 1 in Fig. 3) at the interface. The melting starting time of the stagnation point is a little later than the leftmost node and, the melting completion time of stagnation point for an airfoil simulation is much later than that of the leftmost node.

The differences between airfoil and rectangle simulations may be further delineated by examining the temperature profiles of interfacial nodes at different times for the two simulations. These are presented in Figs. 10 and 11. Comparison of these figures reveals the following:

1) The temperature profiles of interfacial nodes for a rectangular simulation resembles a trigonometric function. The maximum and minimum temperatures are located at interfacial nodes over the centers of the heater and gap, respectively. The difference between the maximum and minimum temperatures is generally less than 5 deg. Only at the time when the interfacial node over the heater center has completed its phase change and the node over the gap center is undergoing phase change does the temperature difference between those two groups of nodes become much larger.

2) For a rectangle simulation, the phase change always starts from the nodes that are positioned over the centers of heaters, then gradually spreads to the nodes that are at the gap center.

3) For an airfoil simulation the temperature profile of interfacial nodes also has features of a trigonometric function, and the maximum and minimum temperature points align with the center of the heater and gap, respectively. However, it differs from the rectangular simulation results in that, the peak occurs on either side of the interfacial points causing the melting interface to move towards node point 1 in Fig. 3. The lowermost temperature value is always at the stagnation point. As can be seen, the temperature of the stagnation point is more than 5 deg lower than the temperature of the sides of the interface before interfacial nodes complete the phase change, and 20 deg lower than other nodes after the interfacial nodes complete the phase change.

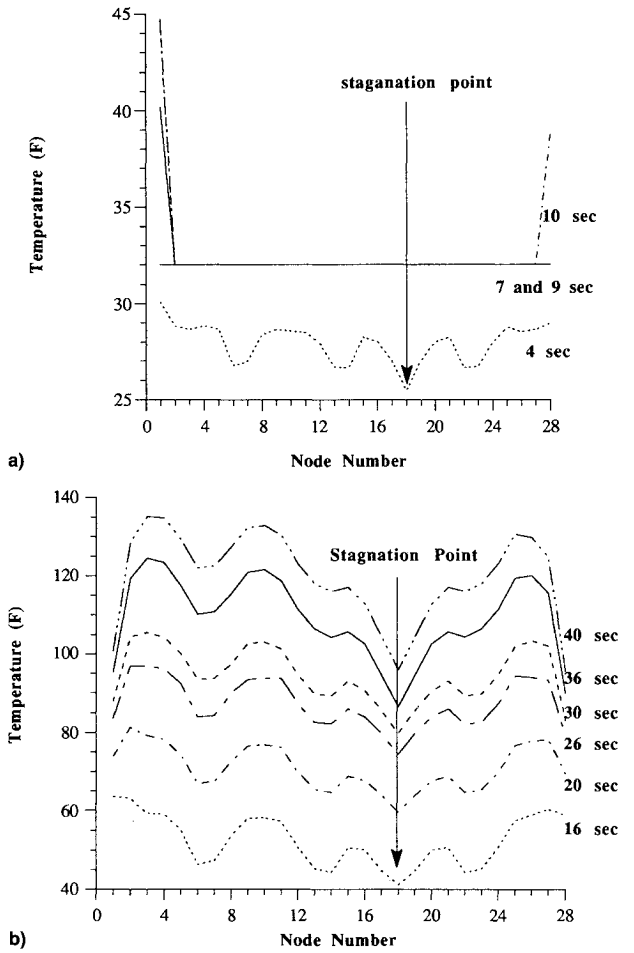

Fig. 11 Temperature profile for interfacial nodes of airfoil for time a) 0–10 and b) 0–40 s.

4) For an airfoil simulation, phase change always starts from the two sides of the interface, then gradually moves toward the center of the interface.

The comparison between the airfoil and rectangle simulations reveals several important differences in the temperature profiles, the temperature history and the melting process. In summary the major differences are as follows:

1) In an airfoil simulation, the temperature at the stagnation point (where curvature is the largest) is lower than the temperatures on either side of it (where curvature is smaller). In the rectangle simulation, the temperature of the node that is over the center of the heater is slightly higher than the temperatures of all other nodes.

2) Melting in the airfoil simulation always starts from the two sides, then gradually moves towards the stagnation position. However, melting in the rectangle simulation occurs almost simultaneously for every node in the same row if the heater gap is small.

3) Comparing the entire melting process, the melting in the airfoil simulation takes longer than that in the rectangle simulation. For the interfacial nodes, the start time of the melting in an airfoil simulation does not differ much from that in a rectangle simulation, usually taking about 0.1–0.5 s longer. However, for the time to complete phase change at the interface or melting time beyond the interfacial nodes, this difference gradually increases and the time delay of the melting for an airfoil simulation becomes more apparent.

Since all the test conditions and physical properties are the same for the two geometries, the only reason for these differences must be attributed to the differences in geometry, or more precisely, the difference in curvature. Obviously, the curvature is closely related to the ratio of ice area/heater area. For the rectangle, this ratio is always equal to one. In other words, the area of the heater is always the same as the ice area. However, for the airfoil the ice area is always larger than the area of the heater since curvature is larger than zero. Therefore, in the airfoil simulation, the unit heater area must affect more of the ice area to make the ice melt sooner than in the rectangle simulation. If the unit heater strength is equal for both simulations, then the ice temperature in the airfoil simulation will be lower than the ice temperature at a corresponding position in the rectangle simulation since it received less heat from the heater. The larger the curvature, the lower the temperature. For the airfoil simulation, the curvature at the stagnation point is the largest, therefore, the temperature of the stagnation point is the smallest. Another important feature for the airfoil surface is the fact that the curvature varies over its entire length. This causes the temperatures of the nodes not to be constant along the surface and creates an inward melting from the two sides of the airfoil towards the stagnation point. After running a number of cases, it has been found that the curvature effect also depends on the thickness of the ice and the distance from the heater to the interface of the ice and substrate. For an airfoil simulation the distance from heater to the interface is usually quite small. Therefore, the curvature effect is not significant for the simulation at an interfacial node if the thickness of ice is small. This can explain why it is difficult to discern the difference in temperature between the simulations of the rectangle and the airfoil for equal test conditions in dry tests (no ice layer). However, if there is ice at the surface of the airfoil, then the curvature effect grows as the thickness of ice increases.

Cylinder Simulation

For the rectangle the curvature is zero everywhere. However, for the airfoil, the curvature along the interface of the airfoil is not constant. At the stagnation point of the airfoil, the curvature is largest, then gradually reduces to zero along the upper and lower surfaces of the airfoil. The curvature varying along the interface of the airfoil causes the interfacial temperature profile in the airfoil simulation to differ from that in the rectangle simulation. The comparison between these two forms of simulations does show the difference, but most of the difference comes from the fact that the curvature of the airfoil varies along the surface. From this kind of comparison it is difficult to see the pure effect of curvature. To isolate curvature effects in the melting process, a set of circular cylinders with different curvatures was analyzed. All test conditions are the same except that the curvature is different for each cylinder. All geometries analyzed have eight layers and six heaters, except in the case of the smallest circular cylinder, which only includes four heaters in order to create large curvature. Figure 12 shows a) a full circular cylinder with four

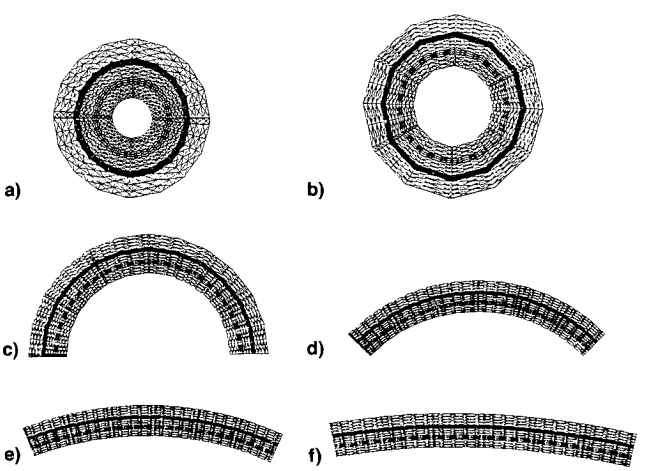

Fig. 12 FEM mesh for cylinders with different curvature.

heaters (curvature = 1.48), b) a full cylinder with six heaters (curvature = 0.9869), c) a half cylinder (curvature = 0.49), d) a quarter cylinder (curvature = 0.25), e) an eighth cylinder (curvature = 0.12), and f) a sixteenth cylinder (curvature = 0.06). Figure 13 shows the rectangular model (curvature = 0). These figures are not plotted to scale in order to save space. In fact, the thickness and total length for all these geometries should be the same except for the circular cylinder with four heaters. Each row of the full circular cylinder has 30 nodes. For the other geometries, each row has 31 nodes. The test conditions are the same as those of the previous problems except heater strengths have been set to 20 W/in.^{2}, and the heaters are turned on for 30 s in every 60-s period of operation. The computed results are shown in Table 2, and temperature histories of interfacial nodes for each geometry are plotted in Figs. 14–20. This comparison gives a quantitative basis for assessing curvature effects. The following major points can be summarized from this comparison:

1) For all geometries, the interfacial nodes begin to change phase at almost the same time, i.e., around 6.1 s. The reason for this is that the distance from the heater to the interface is quite small and that the curvature effect cannot be significant across this small distance.

2) After the interface node begins to change phase, curvature effects become very apparent. For the full cylinder (curvature = 1.48), it takes 1.6 s for all the interfacial nodes to enter the mushy phase, and 6.2 s for all the interfacial nodes to become water. However, for the rectangle (curvature = 0), it takes 0.9 s for all of the interfacial nodes to reach the two-phase state, and 3.3 s for all the interfacial nodes to become water. This indicates that curvature affects the melting process. For geometries whose curvature is larger, it takes a much longer time to complete the phase change.

3) After 60 s, there are 31 + 31 + 27 two-phase nodes and 31 + 27 water nodes for the rectangular geometry. However, there are only 30 + 30 two-phase nodes, and 30 water nodes for the full cylinder with four heaters. This also supports the observation that curvature affects the melting process.

4) The comparison also indicates that when the curvature ratio is less than 0.25, i.e., for the one-quarter, one-eighth, and one-sixteenth cylinders and for the rectangle, the simu-

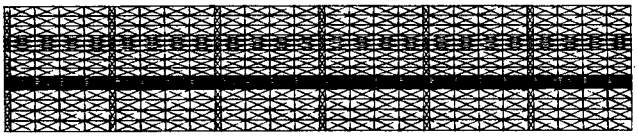

Fig. 13 FEM mesh for reference rectangle (curvature = 0).

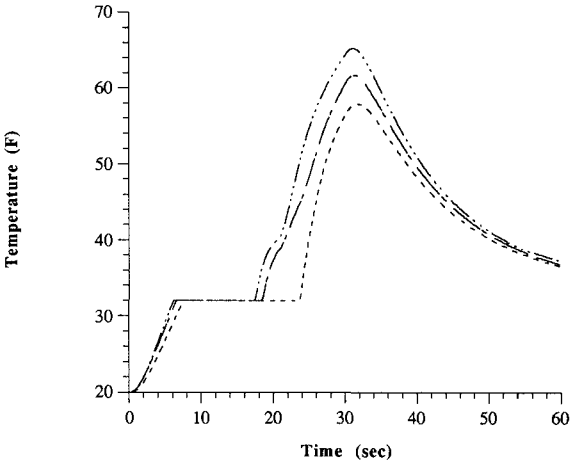

Fig. 14 Temperature history for the interface nodes of a full cylinder with four heaters (curvature = 1.48).

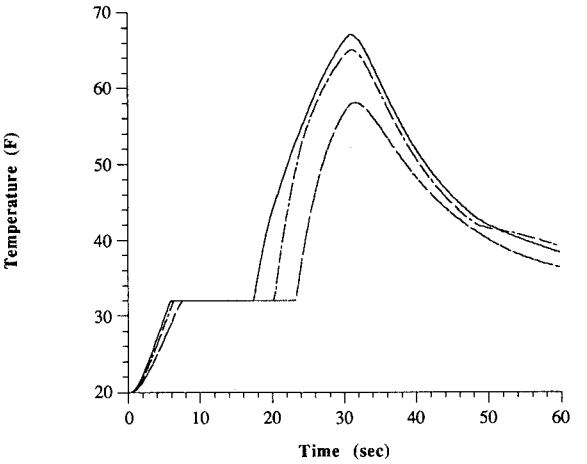

Fig. 15 Temperature history for the interface nodes of a full cylinder with six heaters (curvature = 0.99).

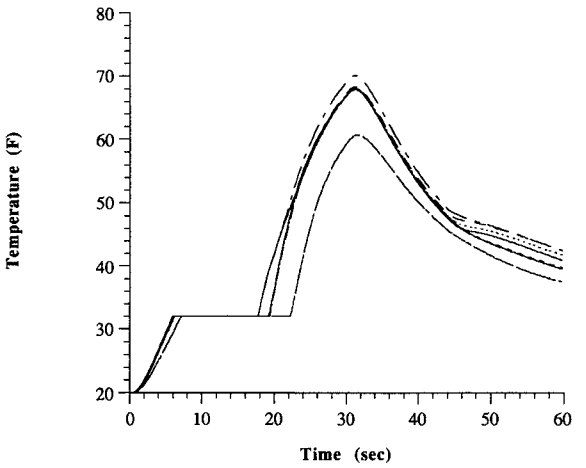

Fig. 16 Temperature history for the interface nodes of a half-cylinder (curvature = 0.49).

Table 2 Comparison of the melting time for cylinders with different curvature

Geometry	Curvature	Melting status of interfacial nodes, s: Two-phase start time	Two-phase complete time	Water start time	Water complete time	No. of two-phase nodes, after 60 s	No. of water nodes, after 60 s
Full cylinder (four heaters)	1.4800	6.1	7.7	17.5	23.7	30 + 30	30
Full cylinder (six heaters)	0.9869	6.1	7.6	17.5	23.3	30 + 30	30 + 12
Half-cylinder	0.4935	6.1	7.2	17.8	22.3	31 + 31 + 7	31 + 28
One-fourth cylinder	0.2467	6.1	7.1	17.9	21.8	31 + 31 + 17	31 + 28
One-eighth cylinder	0.1234	6.1	7.0	18.0	21.6	31 + 31 + 17	31 + 28
One-sixteenth cylinder	0.0617	6.1	7.0	18.0	21.5	31 + 31 + 27	31 + 28
Rectangle	0	6.0	6.9	18.0	21.3	31 + 31 + 27	31 + 28

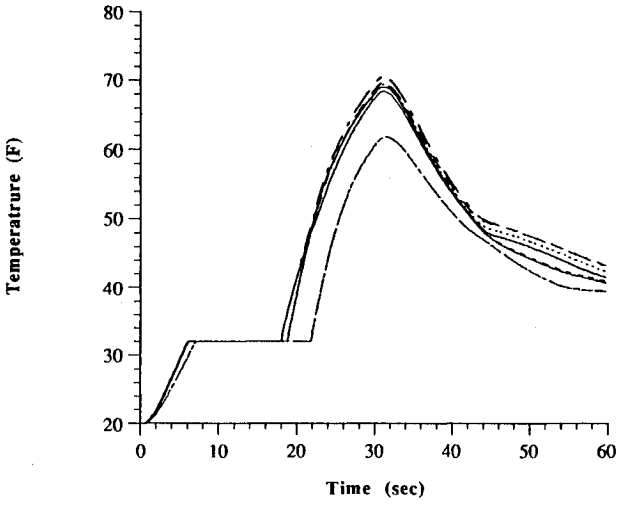

Fig. 17 Temperature history for the interface nodes of a quarter-cylinder (curvature = 0.25).

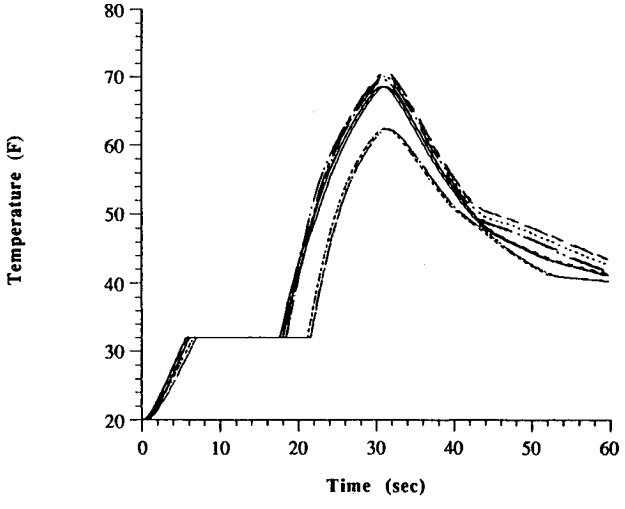

Fig. 18 Temperature history for the interface nodes of a one-eighth cylinder (curvature = 0.12).

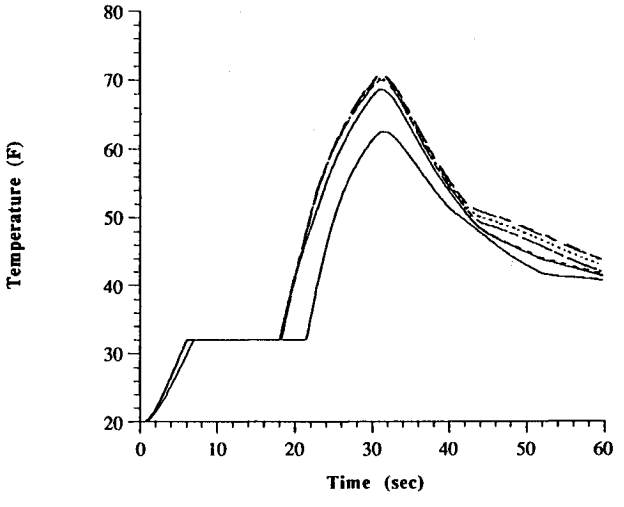

Fig. 19 Temperature history for the interface nodes of a one-sixteenth cylinder (curvature = 0.06).

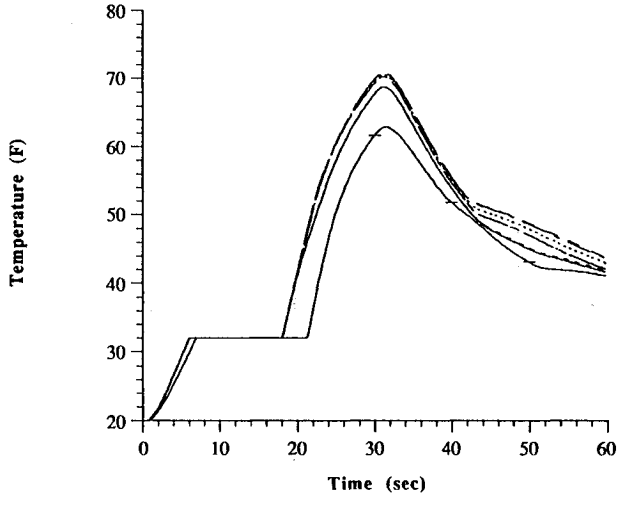

Fig. 20 Temperature history for the interface nodes of a rectangle (curvature = 0).

lation results for those geometries are almost the same. Therefore, a rectangular simulation to model portions of airfoil where curvature is less than 0.25 may be acceptable. However, for the part of the airfoil in which the curvature exceeds 0.9, the actual geometry should be modeled in order to avoid an error for this particular example.

5) Comparing the temperature history of the interfacial nodes (Figs. 14–20), all the curve shapes are very similar (this is expected since the geometric structures are the same and the surface curvatures are constant). But the maximum temperatures for each geometry show some differences. For example, the maximum temperature for the rectangle at its interface after 31 s is 70.9°F compared to: 65.3°F (for the full cylinder with four heaters), 67.0°F (for the full cylinder with six heaters), 70.1°F (for the half cylinder), 70.6°F (for the one-quarter cylinder), 70.7°F (for the one-eighth cylinder), 70.8°F (for the one-sixteenth cylinder), respectively.

The comparisons above indicate that when curvature exceeds 0.9, if a rectangular simulation is used instead of the actual geometry, a significant difference could be produced. For an airfoil, the curvature K at any location can be calculated from

$$K = [y''/(1 + y'^2)^{3/2}] \tag{11}$$

Calculation indicates that the curvature at a typical stagnation point is around 18. Accordingly, the curvature effect at the stagnation point may be even more apparent than the examples above indicate.

Concluding Remarks

1) The results of a simulation of a de-icer pad for an actual airfoil have been compared to the results from a rectangular simulation. The comparison reveals that curvature affects the results in two ways. One is associated with longer melt times for the airfoil model compared to the rectangular model. The other is associated with the melt process: for the airfoil model, melting progresses inwards towards the stagnation point.

2) When the curvature ratio is less than 0.25, the results obtained by using a rectangular simulation are very close to the results of the airfoil simulation for the examples considered in this article. However, at the stagnation point where the curvature has a value of approximately 18, if a rectangular simulation is used to predict the melting process, curvature effects cause a difference in the results.

3) The curvature effect also depends on the thickness of the ice and the distance from the heater to the ice interface. For an airfoil simulation, the distance from the heater to the interface is usually quite small. It was found that the curvature effect is not significant in a simulation in which no ice layer is present. However, for cases with ice on an airfoil surface, the curvature effect is more pronounced for thicker ice layers.

References

[1]Yaslik, A. D., Keith, T. G., Jr., and De Witt, K. J., "Further Developments in Three-Dimensional Numerical Simulation of Electrothermal Deicing Systems," AIAA Paper 92-0528, Jan. 1992.

[2]Henry, R., "Development of an Electrothermal De-Icing/Anti-Icing Model," AIAA Paper 92-0526, Jan. 1992.

[3]Roelke, R. J., Keith, T. G., Jr., De Witt, K. J., and Wright, W. B., "Efficient Numerical Simulation of a One-Dimensional Electrothermal Deicer Pad," *Journal of Aircraft* Vol. 25, No. 12, 1988, pp. 1097–1105.

[4]Henry, R., and Guffond, D., "Infrared Technique to Measure Skin Temperature on an Electrothermal De-Icer, Comparison with Numerical Simulation," AIAA Paper 89-07608, Jan. 1989.

[5]Huang, J. R., Keith, T. G., Jr., and De Witt, K. J., "Numerical Simulation of an Electrothermal De-Iced Aircraft Surface Using the Finite Element Method," AIAA Paper 91-0268, Jan. 1991.

[6]Huang, J. R., Keith, T. G., Jr., and De Witt, K. J., "Efficient Finite Element Method for Aircraft Deicing Problems," *Journal of Aircraft*, Vol. 30, No. 5, 1993, pp. 695–704.

[7]Schneider, G. E., and Raw, M. J., "An Implicit Solution Procedure for Finite Difference Modeling of the Stefan Problem," *Journal of Aircraft*, Vol. 21, No. 11, 1984, pp. 1685–1690.

Recommended Reading from Progress in Astronautics and Aeronautics

Viscous Drag Reduction in Boundary Layers

Dennis M. Bushnell and Jerry N. Hefner, editors

This volume's authoritative coverage of viscous drag reduction issues is divided into four major categories: Laminar Flow Control, Passive Turbulent Drag Reduction, Active Turbulent Drag Reduction, and Interactive Turbulent Drag Reduction. It is a timely publication, including discussion of emerging technologies such as the use of surfactants as an alternative to polymers, the NASA Laminar Flow Control Program, and riblet application to transport aircraft. Includes more than 900 references, 260 tables and figures, and 152 equations.

1990, 530 pp, illus, Hardback • ISBN 0-930403-66-5
AIAA Members $59.95 • Nonmembers $75.95 • Order #: V-123 (830)

Place your order today! Call 1-800/682-AIAA

AIAA
American Institute of Aeronautics and Astronautics

Publications Customer Service, 9 Jay Gould Ct., P.O. Box 753, Waldorf, MD 20604
FAX 301/843-0159 Phone 1-800/682-2422 8 a.m. - 5 p.m. Eastern

Sales Tax: CA residents, 8.25%; DC, 6%. For shipping and handling add $4.75 for 1-4 books (call for rates for higher quantities). Orders under $100.00 must be prepaid. Foreign orders must be prepaid and include a $20.00 postal surcharge. Please allow 4 weeks for delivery. Prices are subject to change without notice. Returns will be accepted within 30 days. Non-U.S. residents are responsible for payment of any taxes required by their government.